forecAsting System for urban heaT Island effect

“Implementation of a forecAsting System for urban heaT Island effect for the development of urban adaptation strategies” (LIFE ASTI)

Action C.4 **Future climate impact assessment of UHI effect and assessmenet of adaption plans**

Thessaloniki January 2021

The project Implementation of a forecAsting System for urban heat Island effect for the development of urban adaptation strategies - LIFE ASTI has received funding from the LIFE Programme of the European Union”.

www.lifeasti.eu

Table of contents

Document Information

Grant agreement number	LIFE17 CCA/GR/OOO108
Project acronym	LIFE ASTI
Project full title	Implementation of a forecAsting System for urban heaT Island effect for the development of urban adaptation strategies
Project's website	**lifeasti.eu**
Project instrument	EUROPEAN COMMISSION - Executive Agency for Small and Medium-sized Enterprises
Project thematic priority	**Climate Change Adaptation**
Deliverable type	Report
Contractual date of delivery	08/2020
Actual date of delivery	01/2021
Deliverable title	UHI Future Climate Assessment Report (UHI-FCAR)
Action	C.4 Future climate impact assessment of UHI effect and assessmenet of adaption plans
Authors	D. Melas, P. Zanis, S. Keppas

Version History

Issue Date	Version	Author	Partner
31-10-2018	V.1	D. Melas, P. Zanis, S. Keppas	AUTh

I Action C4

C4 action has a two-fold objective, which is to a) provide an assessment of the impact of future climate change scenarios on Urban Heat Island (UHI) for the two Mediterranean cities of Thessaloniki and Rome (UHI-FCAR) and b) to assess and quantify the outcome of promoting mitigation measures in the cities mentioned above to reduce/hinder the UHI effect (UHI-ASAR).

The current report refers to the first of the deliverables of the C4 action (Urban Heat Island Future Climate Assessment Report, UHI-FCAR). For the purposes of this subaction/deliverable the climate of a reference and two future periods has been simulated via the Weather Research Forecast (WRF) mesoscale meteorlogical model, which was used as a Regional Climate Model (RCM).

The present document describes the future climate impact on the UHI effect and the methodologies applied to produce such results. In particular, the current document referes to:

1) the modelling system's set up (configuration of the domains, schemes etc);
2) the results.

1) Modelling system's set up

a) Domains

For the purposes of the current action, the WRF model has been applied over four (2-way) nested domains with spatial resolutions of 50km (d01), 10km (d02) and 2km (d03, d04) (**figure 1**). The first domain (d01; mesh size of 166x98) covers most of the Europe, the North Africa and the Middle East to simulate the synoptic meteorological conditions. The second domain (d02; mesh size of 55x43) includes the eastern Mediterranean, while two smaller domains within the d02 focus on the studied urban areas of Thessaloniki, Greece (d03; mesh size of 16x16) and Rome Italy (d04; mesh size of 16x16). The vertical profile of all the domains is composed of 35 unevenly spaced full sigma layers (between ~35m and 100hPa). In order to understand the topography of the fine resolution domains d03 and d04, figure 2 depicts the altitude over these regions.

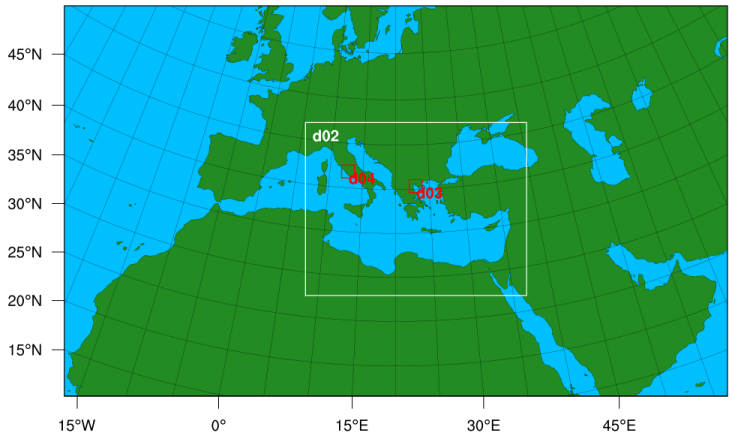

Figure 1. Configuration of the four (2-way) nested WRF modeling domains

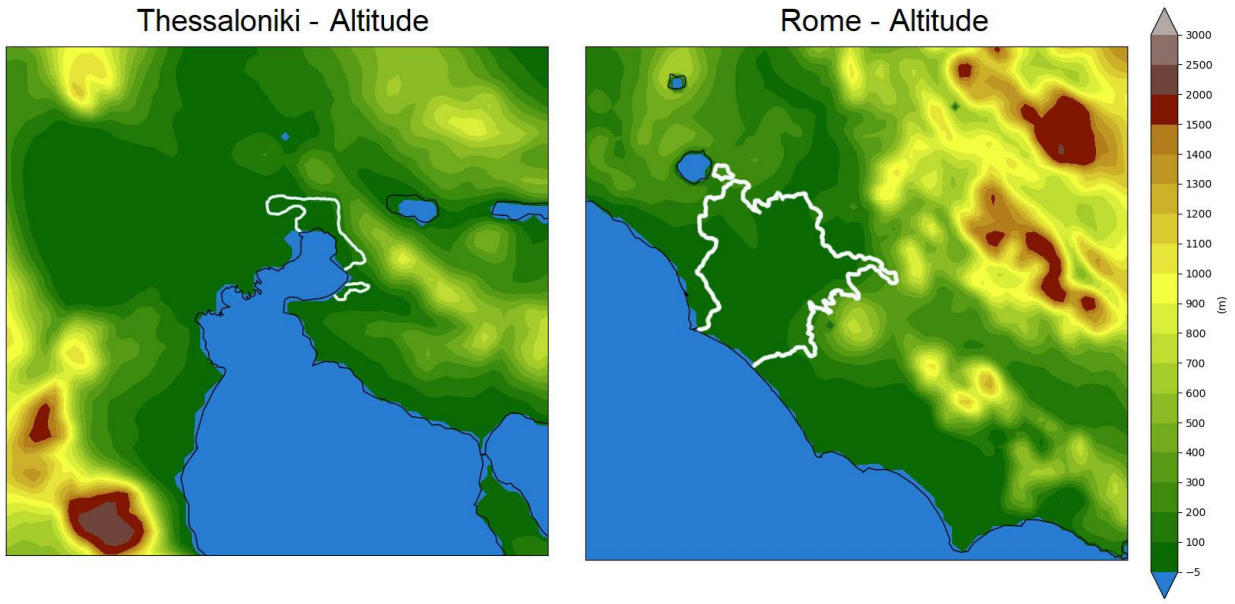

Figure 2 – Altitude maps for the domains d03 (Thessaloniki - left) and d04 (Rome - right). White contour shows indicates the urban area.

b) Simulation periods and the boundary conditions

Three simulations were performed in total over different periods. The first period is the so called reference period (2006-2010), which is used as a representative period of the current climate. The rest of the simulations refer to the periods 2046-2050 and 2096-2100, which were selected in order to obtain the climate at both the middle and the end of the current century over the study area. For the rest of this report, periods 2006-2010, 2046-2050 and 2096-2100 will be referred as periods A, B and C respectively.

The lateral boundaries, which were used by the model for both the simulations of both the control and the future periods, were obtained from the National Center for Atmospheric Research (NCAR). The datasets include global bias-corrected climate model output data from version 1 of NCAR's Community Earth System Model (CESM1) that participated in phase 5 of the Coupled Model Intercomparison Experiment (CMIP5), which supported the Intergovernmental Panel on Climate Change Fifth Assessment Report (IPCC AR5). All variables needed for initial and boundary conditionsare included, and have been bias-corrected using the European Centre for Medium-Range Weather Forecasts (ECMWF) Interim Reanalysis (ERA-Interim) fields for 1981-2005, following the method in Bruyere et al. (2014). The data are interpolated to 26 pressure levels, have a horizontal resolution of approximately 1° and are provided in files at six hourly intervals. The dataset that was used for the current action refers to the Representative Concentration Pathway (RCP) future scenario 8.5. In this scenario the greenhouse gas emissions and concentrations increase considerably over time, leading to a radiative forcing of 8.5 W m^{-2} at the end of the current century.

c) Physics options

The WRF physics schemes include: (a) microphysics, (b) cumulus physics, (c) planetary boundary and surface layer parameterizations, (d) land surface physics, and (e) short-wave and long-wave radiation parameterizations. Each category has multiple options varying from simple and efficient to more sophisticated and computationally costly. A considerable effort of research has been implemented over the LIFE ASTI project studied regions examining the WRF performance in replicating hot summer conditions and the UHI effect (Giannaros T.M. and Melas, 2012, Giannaros T.M. et al., 2014; Giannaros C. et al., 2018, 2019; Morini et al., 2017). Based on these studies but also taking into account the computational cost, the physics parameterizations listed in **Table 1** will be applied in all modeling domains of the LIFE ASTI forecasting system.

Physics	Parameterization	References
Microphysics (clouds)	WRF single-moment 6-class (WSM6)	Hong and Lim (2006)
Cumulus (convection)*	Kain-Fritsch (KF)	Kain (2004)
Planetary boundary layer	asymmetric convection model 2 (ACM2)	Pleim (2007a, 2007 b)
Surface layer	Monin-Obukhov (Janjic Eta) scheme	Monin and Obukhov (1954); Janjic (1996)
Land surface	Noah model	Tewari et al. (2004)
Short-wave radiation	RRTMG	(Iacono et al. 2008, JGR)

* Cumulus parameterization will be used only for domains d01 and d02

Table 1. Summary of the WRF physics options

d) Land use/land cover

For the representation of the land use/land cover (LULC) in the WRF model, two differerent datasets were used. For the domains d01 and d02, the Global Land Cover by National Mapping Organizations (GLCNMO) was used (Tateishi, 2011; Hua et al., 2018). This dataset has a resolution of 30 archseconds and includes 20 different LULC classes (**table 2**). However, for the urban-scale domains d03 and d04, LULC was obtained from the 250m spatial resolution CORINE 2012 dataset (version 18.5.1) that includes 44 LULC categories (**table 3**) (Büttner, 2014). As shown in **table 3**, the CORINE data enable the three additional urban LULC categories (IC, HIR, LIR) that are necessary for implementing the Single Layer Urban Canopy Model (SLUCM) (Giannaros C, 2018). **Figure 2** demonstrates the land use classes over the domains d03 (Thessaloniki) and d04 (Rome). The pinkish and greyish colours indicate the urban areas.

Code	Class Name	Code	Class Name
1	Broadleaf Evergreen Forest	**11**	Cropland
2	Broadleaf Deciduous Forest	**12**	Paddy field
3	Needleleaf Evergreen Forest	**13**	Cropland / Other Vegetation Mosaic
4	Needleleaf Deciduous Forest	**14**	Mangrove
5	Mixed Forest	**15**	Wetland
6	Tree Open	**16**	Bare area,consolidated(gravel,rock)
7	Shrub	**17**	Bare area,unconsolidated (sand)
8	Herbaceous	**18**	Urban
9	Herbaceous with Sparse Tree/Shrub	**19**	Snow / Ice
10	Sparse vegetation	**20**	Water bodies

Table 2. Summary of the GLCNMO classes.

CORINE urban LULC classification	MODIS/IGBP urban LULC classification
1.1.1: Continuous urban fabric	32: High-intensity residential
1.1.2: Discontinuous urban fabric	31: Low-intensity residential
1.2.1: Industrial/commercial units	33: Industrial/commercial
1.2.2: Road/rail networks and associated land	13: Urban and built-up
1.2.3: Port areas	13: Urban and built-up
1.2.4: Airports	13: Urban and built-up
1.3.1: Mineral extraction sites	13: Urban and built-up
1.3.2: Dump sites	13: Urban and built-up
1.3.3: Construction sites	13: Urban and built-up
1.4.1: Green urban areas	31: Low-intensity residential
1.4.2: Sports and leisure facilities	31: Low-intensity residential

Table 3. Mapping strategy of the CORINE urban LULC elements to the corresponding WRF urban LULC categories

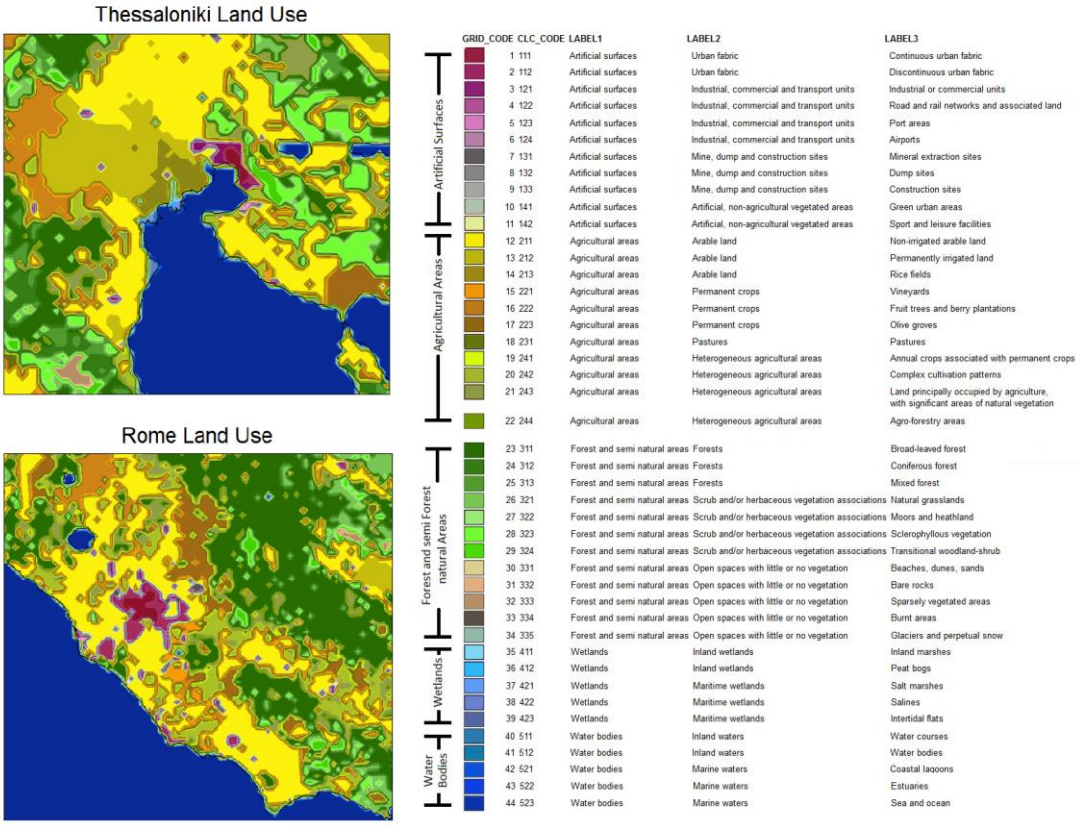

Figure 2 – Land use classes over the domains 03 (Thessaloniki - up) and 04 (Rome - down) as considered in the CORINE 2012 dataset.

2) Results

The simulations for the reference and the two future 5-year periods results are described and compared in the next subsections. As the LIFE-ASTI programme focuses on the UHI, variables such as temperature, heating/cooling degree days and urban heat island intensity are discussed for the two cities of interest, Thessaloniki and Rome.

a) Thessaloniki

For the domain d03 of Thessaloniki, the annual average temperature for the reference period is ~17.5°C. The expected temperature increase is of the order of 1°C and ~3.5°C for the periods 2046-2050 and 2096-2100, respectively (**figure 3**). Focusing on the greater area of Thessaloniki (thus, the entire urban area and the rural areas close by the city), it can be noticed that the southeastern regions located relatively far from the coastline (>6km) present a trend of further temperature increase compared to the northwestern regions during summertime. In particular, this increase is much more intense during Spring (+0.7°C and +3.8°C for periods B and C) and Summer (+1.4°C and +4.4°C) in the southeast, while in the northwest the expected increase is slightly lower (+0.6°C, 3.6°C and +1.2°C, +4.2°C respectively). During autumn and winter there is no significant trend in the temperature over the entire urban region.

As the project focuses on the urban heat island and the way that the climate change affects it, **figure 5** presents a comparison between three urban and two reference points (**figure 4**). The three urban points were selected in order to represent the centre of the city (CU) and the centre of the west (WU) and east (EU) urban area. In addition, the 2 reference points are representatives of the west (WR) and east (ER) ambient rural areas. In general, for the period A, the WR point exhibits the lowest minimum average temperatures through the year (average annual is ~17.5°C), but also the highest maximum average values during summer (31.5°C).The ER point is usually up to 1°C warmer than WR. Regarding the urban points (CU, WU, EU), the temperature during the night is higher by 2-3°C through the year, while, during the day, the temperature difference between urban and reference points is between <+0.5°C to ~ +1°C. In average, by the year 2050 (2100) in these five selected points the temperature is expected to increase by 0.8°C (2.7°C), 0.6°C (3.7°C), 1.3°C (4.1°C) and 1.7°C (4.2°C) in winter, spring, summer and autumn, respectively. Finally, the temperature seems to increase more during the afternoon (by ~+0.2°C comparing to the other periods of the day) in winter and spring, while in summer the maximum increase is expected early in the morning (up to ~+0.4°C comparing to the other periods of the day).

Moving to **figure 6**, during the reference period early in the morning (0-3UTC), the UHI intensity between urban and west (urban and east) is ~2°C (~1°C) reference points in winter, while in summer the intensity increases ~3°C (~2°C) on average. However, in the afternoon the UHI effect is practically eliminated. Regarding the future periods, there are no significant changes in the UHI effect. An interesting finding could be the increasing trend of the UHI effect in summer for the eastern regions at 12-18UTC by +0.1°C and 0.4°C, which is caused (taking into account figure 3) by a more intense increase of the temperature over the eastern rural area.

Regarding the energy consumption, **figure 7** indicates (as expected) that energy demand for heating will decrease in winter. In contrast, cooling degree days will increase in the summer. In particular, the winter average heating degree days (HDD) for the reference period is 5-7°C, which is expected to decrease by 0.85°C and 2.6°C by the year 2050 and 2100. This change seems to be uniform over the majority of lower ground areas in the domain. However, looking at the summer average cooling degree days, it seems that for the reference period this parameter fluctuates between 3-5°C over the urban area of Thessaloniki. This footprint of the city differs by 2°C or more from the areas around it. By the year 2050, CDD is expected to increase by 1.2-1.5°C, while by the year 2100, this increase will reach 4-4.4°C. It should be hihglighted that the eastern regions of the city demonstrate the highest increase.

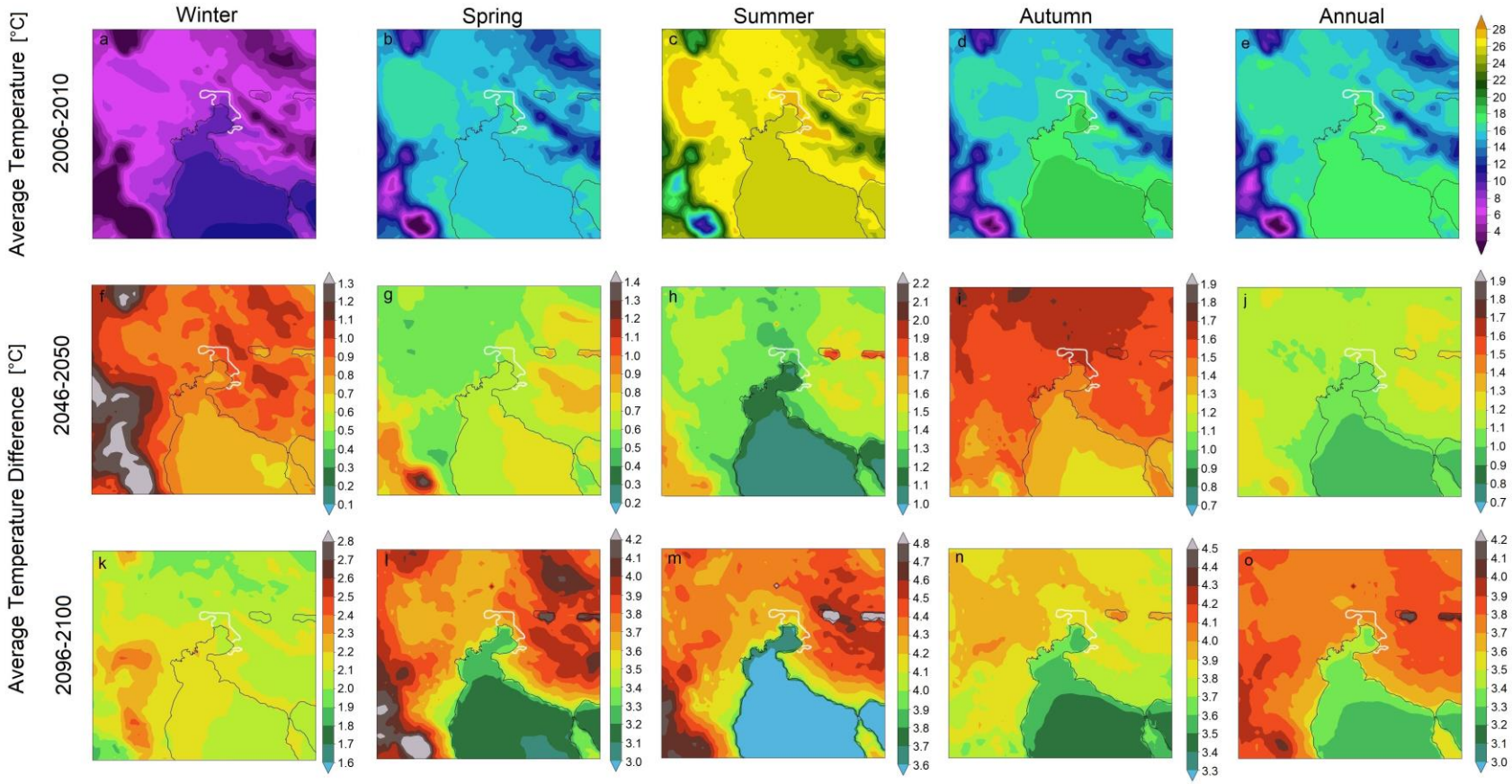

Figure 3 – Figures a-e show the winter, spring, summer, autumn and annual average temperature for the period A (2006-2010). Figures f-j show the temperature difference betweeen the periods 2046-2050 and 2006-2010 for the different seasons of the year. Figures k-o are similar to f-j, but for the periods 2096-2100 and 2006-2010. The white line is used to depict the boundaries of the urban area.

Point	Location	Land Use	Elevation (m)
CU	Ancient Roman Market	Continuous Urban Fabric	91
WU	Evosmos	Continuous Urban Fabric	15
EU	Pylea	Continuous Urban Fabric	57
WR	Anatoliko	Non-irrigated arable land	4
ER	Epanomi	Non-irrigated arable land	77

Figure 4 – The selected reference and urban points in the domain 03 for the city of Thessaloniki.

Finally, in **figure 8**, we indicatively present the apparent temperature (TAPP) calculated for the typicaly warmer month of the year (July) for d03 as a function of temperature (T in °C) and dew point temperature (Tdew in °C) by the following equation to represent the thermal discomfort on local poluations:

$$\mathrm{TAPP} = -2.653 + 0.994 \cdot \mathrm{T} + 0.0153 \cdot (\mathrm{Tdew})^2) \text{ (Kalkstein et al., 1995) (Eq. 1)}$$

Epidemiological studies have shown a typical J-U-shaped association between temperature indicators, such as TAPP, and health outcomes such as mortality and hospital admission during summer, with a non-linear increase in daily deaths/admissions as temperatures rise above the threshold value (Curriero et al 2002, Kovats and Hajat, 2008; Benmarhnia et al. 2015).). Under current climatic conditions (**figure 8a, 9a**), TAPP presents increased values (24-26°C) close to the sea and lakes early in the morning, while in the afternoon maximum TAPP (~33°C) is observed in low ground regions far from the sea. This can be explained by the fact that temperature and humidity usually present a narrow diurnal range at places close by the sea, especially under anticyclonic conditions. Instead, in continental areas far from the sea these variables exhibit a larger range. Exceptions are some parts of the city of Thessaloniki, which although are located next to the sea, exhibit TAPP ~31-32°C due to the urban environment. In the future,

changes are expected in minimum TAPP, which is important as nightime cooling enables us to recover from daily heat exposure and can affect quoaity of our sleep (Lan et al., 2014; Joshi et al., 2016; Lan et al., 2017). It should be noted that in average, in d03, TAPP will increase by 2-3°C and 4-5°C by 2050 and 2100 respectively both during early morning (03UTC) and early afternoon (12UTC) in July (**figure 8d, g and 9d, g**). However, lower ground areas will have higher TAPP (~+0.5°C) compared to ambient elevated regions. Regarding the city of Thessaloniki, major increases are expected at the very west and east parts, and especially at the southeastern parts. In particular, average TAPP at 03UTC will increase by 2.5°C and 4.9°C by 2050 and 2100, while the average increase at 12UTC will be of the order of 2°C and 4.5°C respectively. Taking into account the eq. 1, it seems that TAPP calculation is mostly based on the temperature rather than the dew point. Hence, although dew point increases at both 03 and 12UTC, during 2046-2050 (**figures 8e-f and 9e-f**), by almost 1°C more than the temperature (this occurs mostly over the city and further to the east), the contribution of the temperature increase is still more significant. For the period 2096-2100, the temperature increase is more significant (+3.4°C) than the dew point (+2.4°C) in the urban area and it is still the factor that contributes to the TAPP increase the most (**figures 8h-i and 9h-i**).

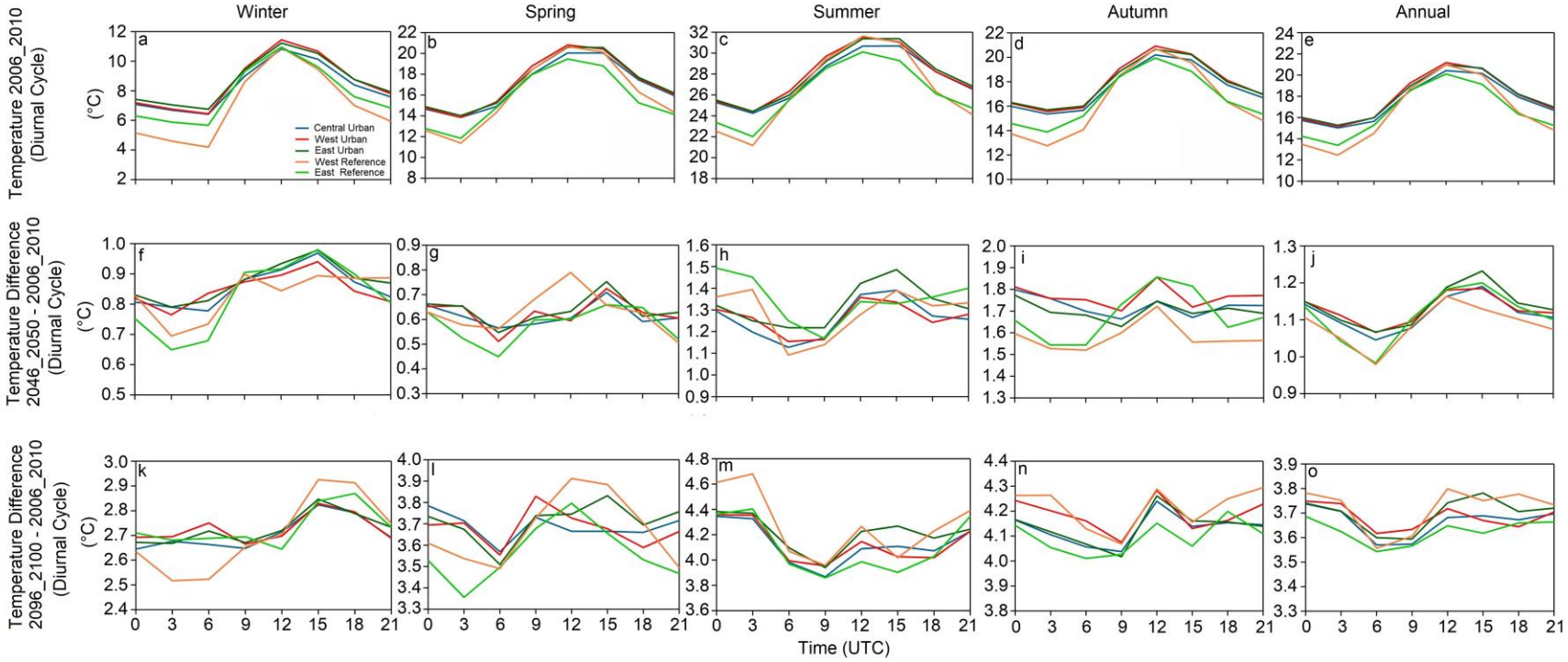

Figure 5 – Figures a-e show the diurnal temperature cycle for the five selected points of the domain of Thessaloniki (figure 4). Figures f-j show the temperature difference betweeen the periods 2046-2050 and 2006-2010 for the different seasons of the year. Figures k-o are similar to f-j, but for the periods 2096-2100 and 2006-2010.

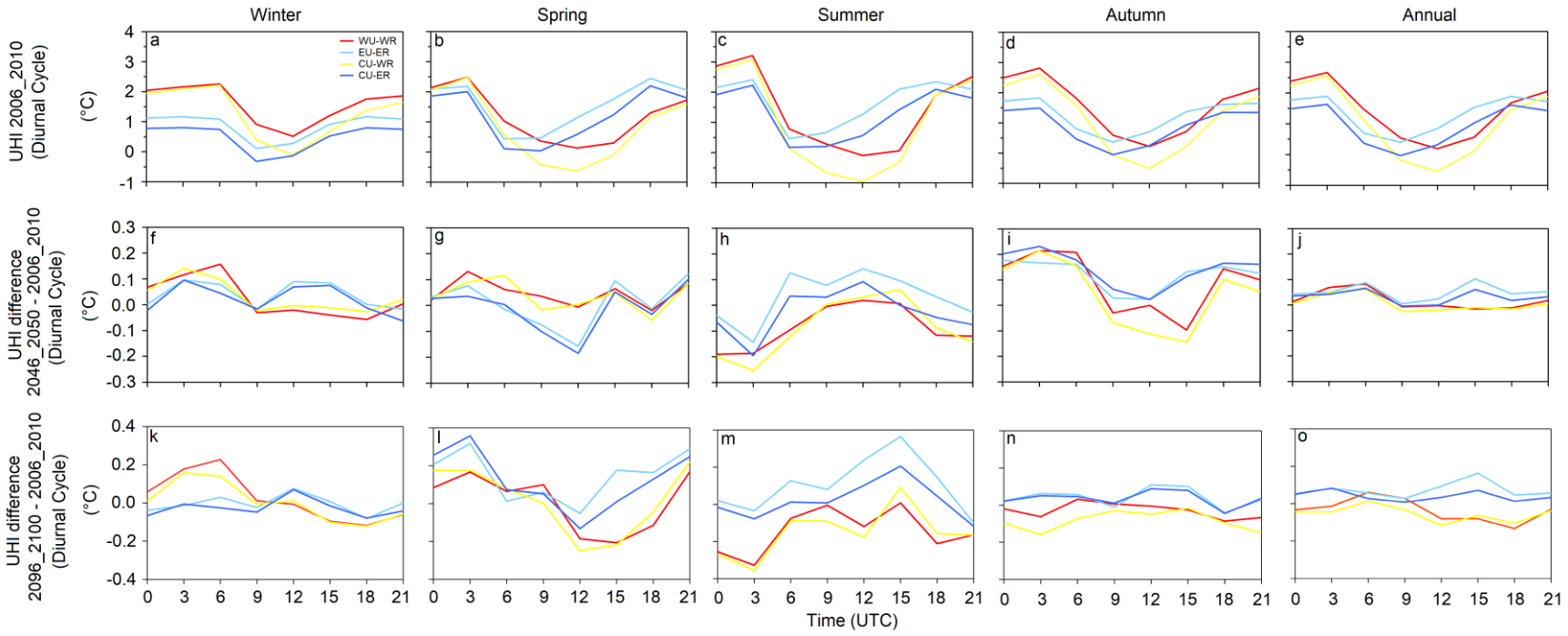

Figure 6 – Figures a-e show the diurnal urban heat island intensity as calculated between WU-WR, EU-ER, CU-WR and CU-ER points of the domain of Thessaloniki (figure 4). Figures f-j show the UHI effect difference for the different seasons of the year betweeen 2046-2050 and 2006-2010. Figures k-o are similar to f-j, but for the periods 2096-2100 and 2006-2010.

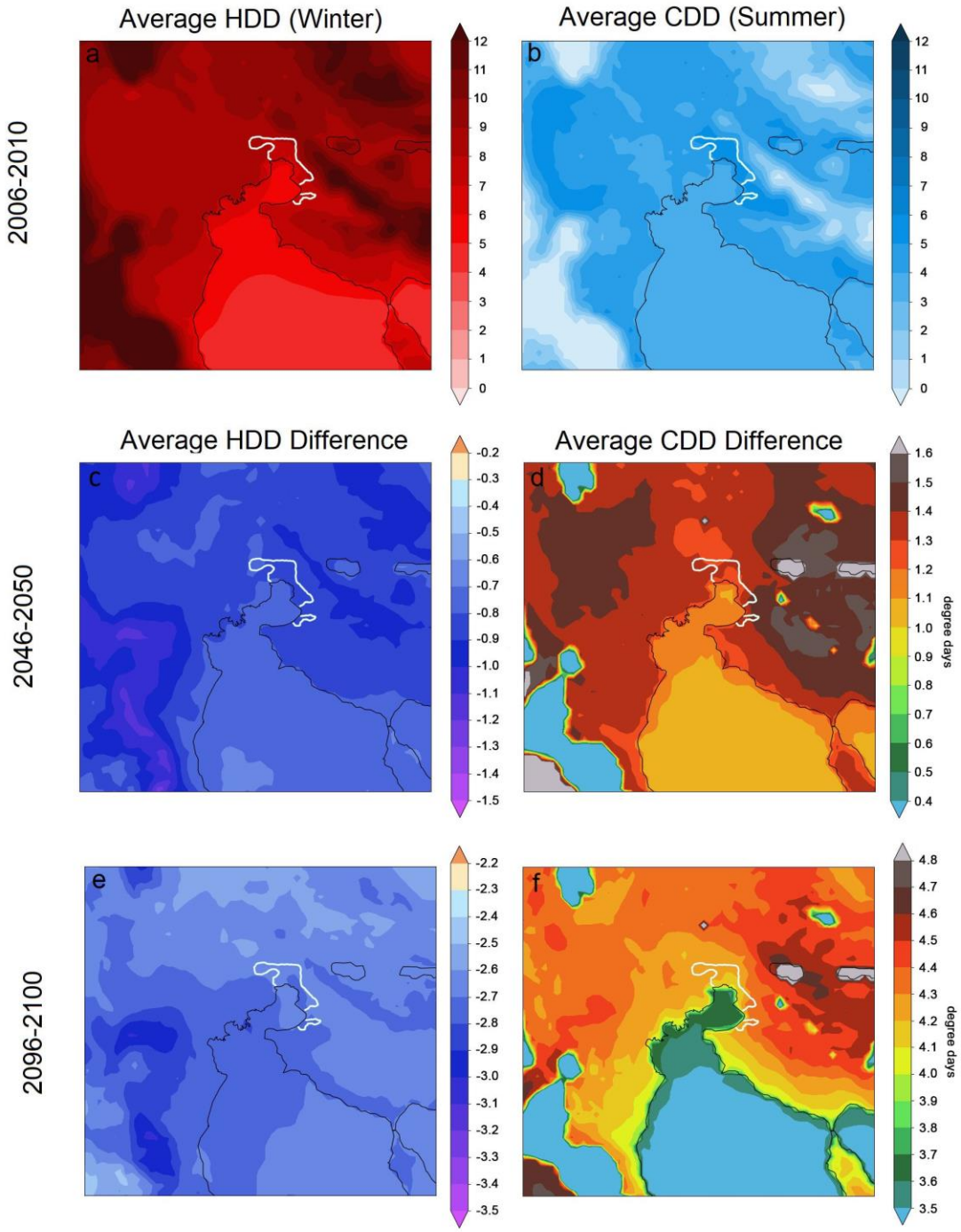

Figure 7 – Average Heating and Cooling Degree Days for winter and summer respectively for the reference period (a, b). Figures c,d and e,f show the HDD and CDD difference between the periods 2046-2050 and 2096-2100 with respect to the reference period. The white line is used to depict the boundaries of the urban area of Thessaloniki.

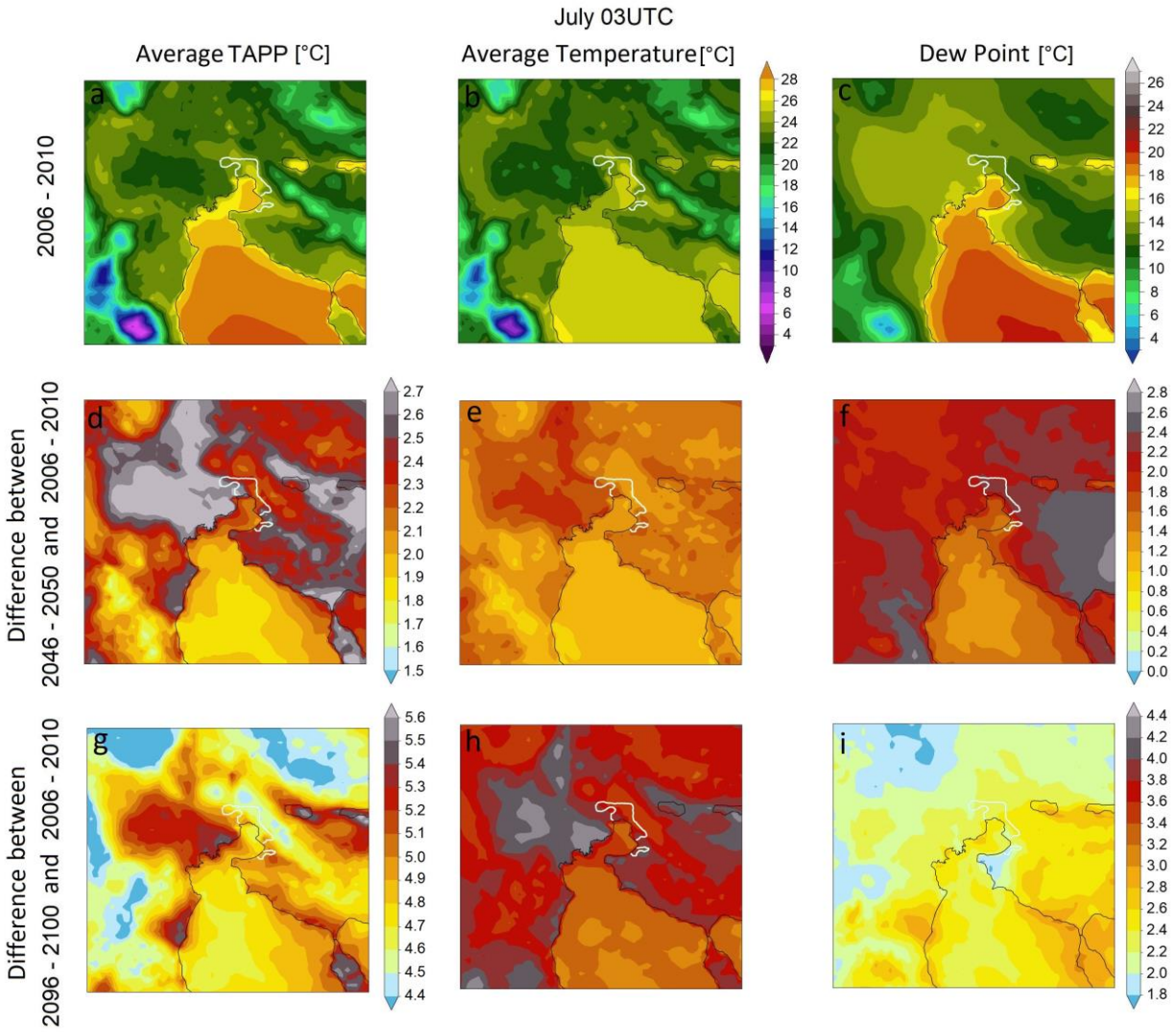

Figure 8 – Average apparent temperature (TAPP) in °C for July at 03UTC, respectively, for the reference period (a, b). Figures d-f and g-i show TAPP difference between the periods 2046-2050 and 2096-2100 with reference, respectively. The white line is used to depict the boundaries of the urban area of Thessaloniki. Figures a-b, e-f and h-i share the same colourscales respectively.

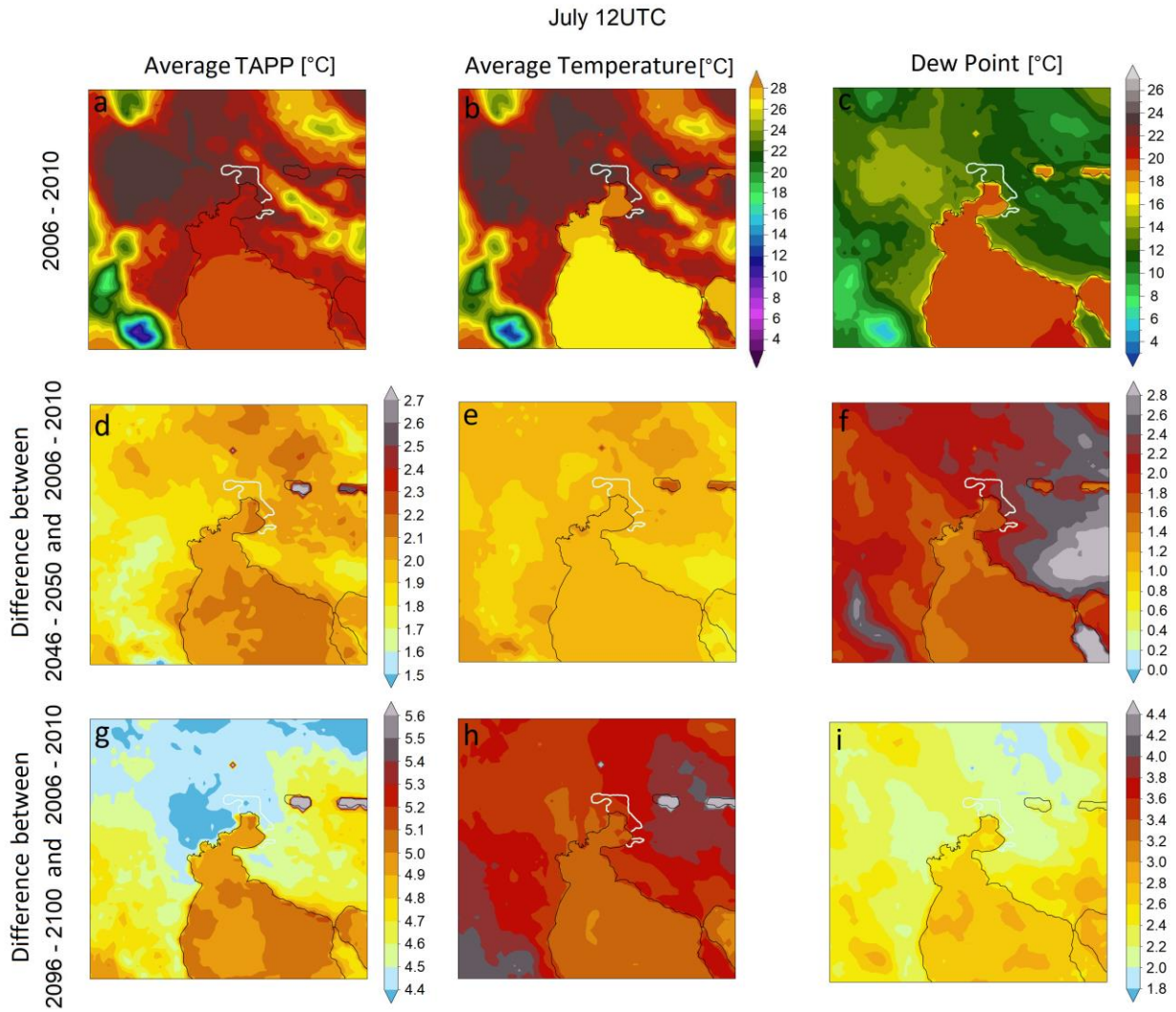

Figure 9 – Average apparent temperature (TAPP) in °C for July at 12UTC, respectively, for the reference period (a, b). Figures d-f and g-i show TAPP difference between the periods 2046-2050 and 2096-2100 with reference, respectively. The white line is used to depict the boundaries of the urban area of Thessaloniki. Figures a-b, e-f and h-i share the same colourscales respectively.

b) Rome

For the domain d04 of Rome, the annual average temperature for the reference year is ~17°C. The expected temeperature increase is of the order of 1°C and ~3.4°C for the periods 2046-2050 and 2096-2100, respectively (**figure 10**). The largest temperature increases compared to the present are expected in summer (+1.4 and +4°C in the middle and the end of the current century) and the lowest during the winter (+0.5 and +2°C, respectively). Focusing on the greater area of Rome (thus the entire urban area and the rural areas close by the city), it can be noticed, as a general trend, that the further the distance to the sea, the largest the temperature increase in the future. The temperature increase difference between a region at the west (by the sea) and another at the east of the city of Rome is on an annual basis of a an order of 0.3°C and 0.7° for periods 2046-2050 and 2096-2100, respectively. The largest differences between west and east regions are observed during summer and autumn (up to 0.7°C), while the lowest ones (0.3°C) are noticed during winter and spring for the period 2046-2050. However, along the period 2096-2100, the temperature increase difference is greater for spring, summer and autumn (0.7-1°C), while during the winter this difference remains low (~0.3°C).

Regarding the urban heat island and the way that the climate change affects it, **figure 11** displays a comparison between three urban and two reference points (**figure 12**) in a pattern similar to that followed for Thessaloniki. The three urban points were selected in order to represent the centre of the city (CU) and an urban area at the west (WU) and east (EU) of the city of Rome. In addition, the two reference points are representatives of the west (WR) and east (ER) ambient rural areas. In general, for the period A, the WR point exhibits the lowest minimum average temperatures through the year (average annual is ~16.5°C), and the lowest maximum average values during summer (28°C). The ER point is usually up to 1°C warmer than WR. Regarding the urban points (CU, WU, EU), the temperature during the night is higher than this in reference points by ~2°C through the year, while, during the day, the temperature difference between urban and ER point is eliminated. It should be noted that the WR point remains cooler especially during Spring and Summer in the afternoon as it is located close to the coastline. In average, the temperature is expected to increase, by the year 2050 (2100), by 0.5°C (2°C), 0.4 °C (3.7°C), 1.2°C (4°C) and 1.4°C (3.6°C) in winter, spring, summer and autumn respectively in these five selected points. Finally, regarding the temperature diurnal cycle, there is no significant trend of temperature change at a specific period of the day.The most noteable are the warmer afternoons during the winter by the year 2050 (by 0.2°C comparing to the rest of the day) and the warmer spring afternoons by the end of the century (by 0.3°C comparing to the rest times of the day).

Moving to **figure 13**, during the reference period in the night and morning (18-06UTC), the average UHI intensity is ~2-2.5°C (~1-1.5°C) between urban and west (east) reference points through the entire year. However, in the afternoon the UHI effect between urban and east reference points is practically eliminated, while between urban and west remains at ~2°C almost all times of the day. Regarding the future periods, there are no significant changes in the UHI effect except for the spring period, when the UHI intensity seems to be slightly enhanced (by 0.2-0.3°C) during the afternoon.

Finally, **figure 14** indicates (as expected) that energy consumption for heating will decrease in winter. In contrast, cooling degree days will increase in the summer. In particular, the winter average heating degree days (HDD) for the reference period is 4-6 degree days , which is expected to decrease by 0.5 and 1.8 degree days by the year 2050 and 2100 in Rome and the regions around. This change seems to be uniform over the majority of lower ground areas in the domain, especially during the winter. On the other hand, the CDD during the reference period is ~3-4 degree days, increasing by 1.1 and 4.1 degree days by 2050 and 2100, respectively.

Finally, in **figures 15 and 16** we present the apparent temperature (TAPP; see Eq. 1). In the present climate, TAPP presents increased values (24-26°C) close to the sea and lakes early in the morning (03UTC), while in the afternoon maximum TAPP (~32°C) is observed in low ground regions far from the sea. The central and northeastern parts of the city of Rome for both time periods seem to exhibit the highest TAPP (24°C and 32°C respectively) presenting a high TAPP city signature in the map (**figure 15a and 16a**). Similarly to d04, although TAPP for the entire domain will increase on average by 2-3°C and 4-5°C by 2050 and 2100, respectively, in lower ground areas TAPP increase will be

much more intense (by ~+0.4°C to +1°C) than that in elevated regions at both 03 and 12 UTC. The city of Rome exhibits the largest increases, +2.6°C and +5.6°C by the middle and the end of the century (**figure 15d,g and 16d,g**). It is worth mentioning that at the end of the current century TAPP will be much higher at 03UTC (by up to 1°C), reaching pratically average values of >30°C for the month of July. Again, TAPP is mostly affected by the temperature increase. In the case of the domain of Rome, temperature increase seems to be larger than dew point in both future periods (**figures 15 and 16b-c, e-f, h-i**). In particular, temperature over the urban area at both 03 and 12UTC exhibits an increase of ~2.2°C and ~3.6-4°C in 2050 and 2100 periods respectively, while dew point increases by 1.6°C and 2.6-3.2°C. It should be noted that dew point increase tend to be larger over the western coastal area and Rome at 03UTC and lower at 12UTC. This may show that dew point increase contributes more to the TAPP increase during the morning.

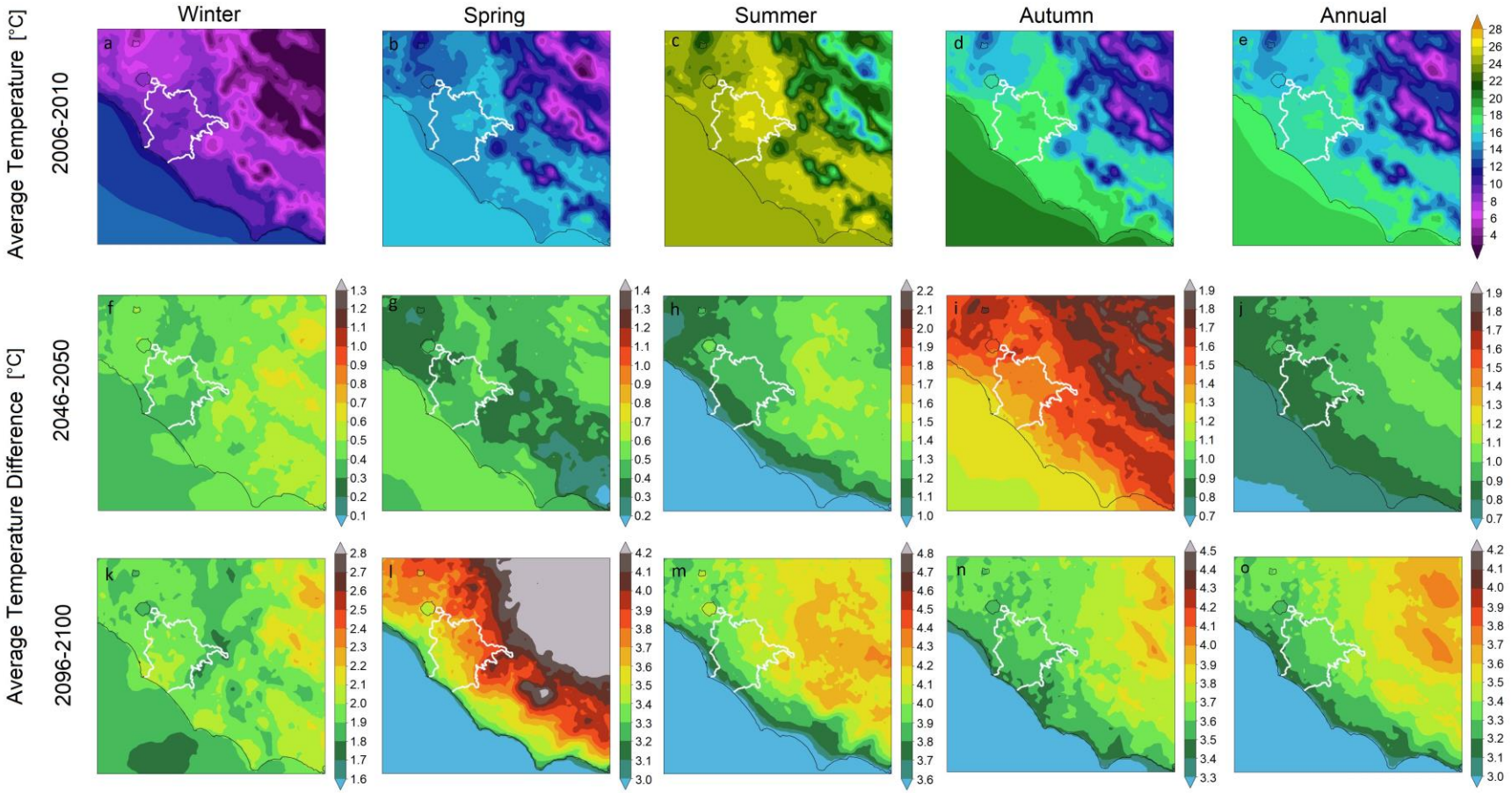

Figure 10 – Same as figure 3, but for domain 04 of Rome.

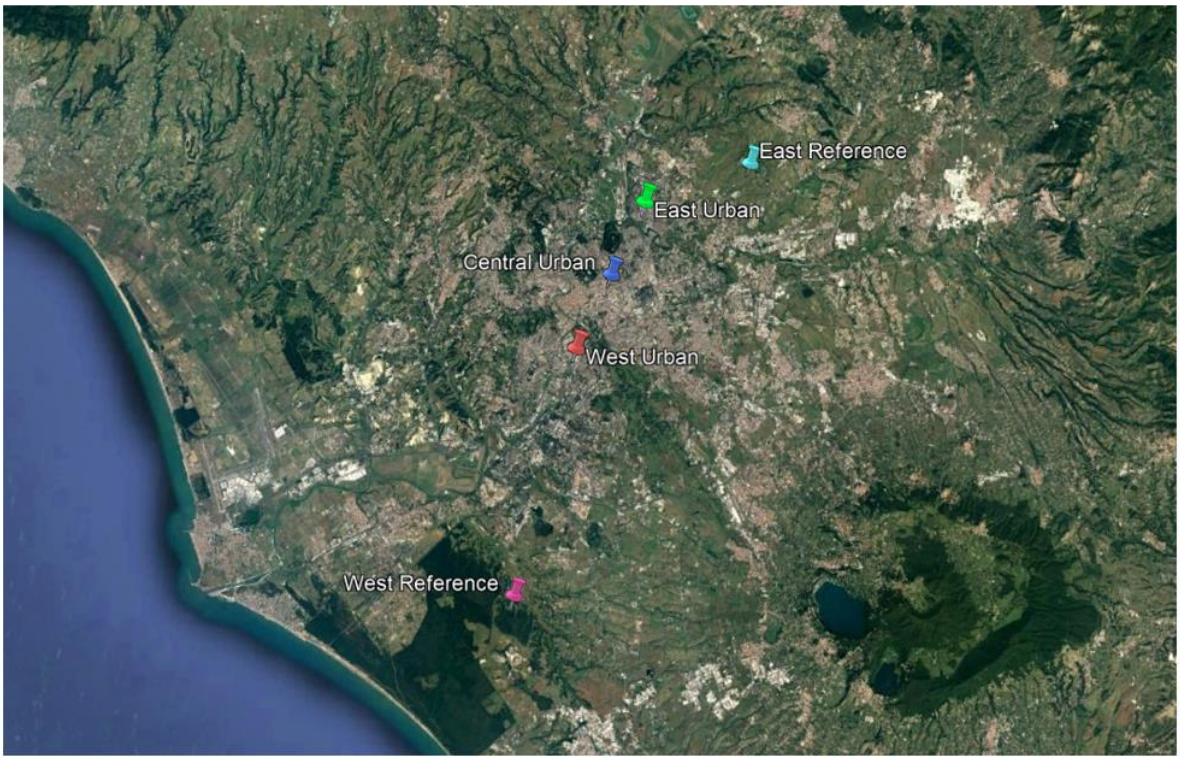

Point	Location	Land Use	Elevation (m)
CU	Central Stazione Termini	Continuous Urban Fabric	55
WU	Silvio d'Amico	Continuous Urban Fabric	31
EU	Viale Jonio	Continuous Urban Fabric	37
WR	Selcetta	Land principally occupied by agricultire, with significan areas of natural vegetation	21
ER	Bufallota	No-irrigated arable land	12

Figure 11 – Same as figure 4, but for domain 04 of Rome.

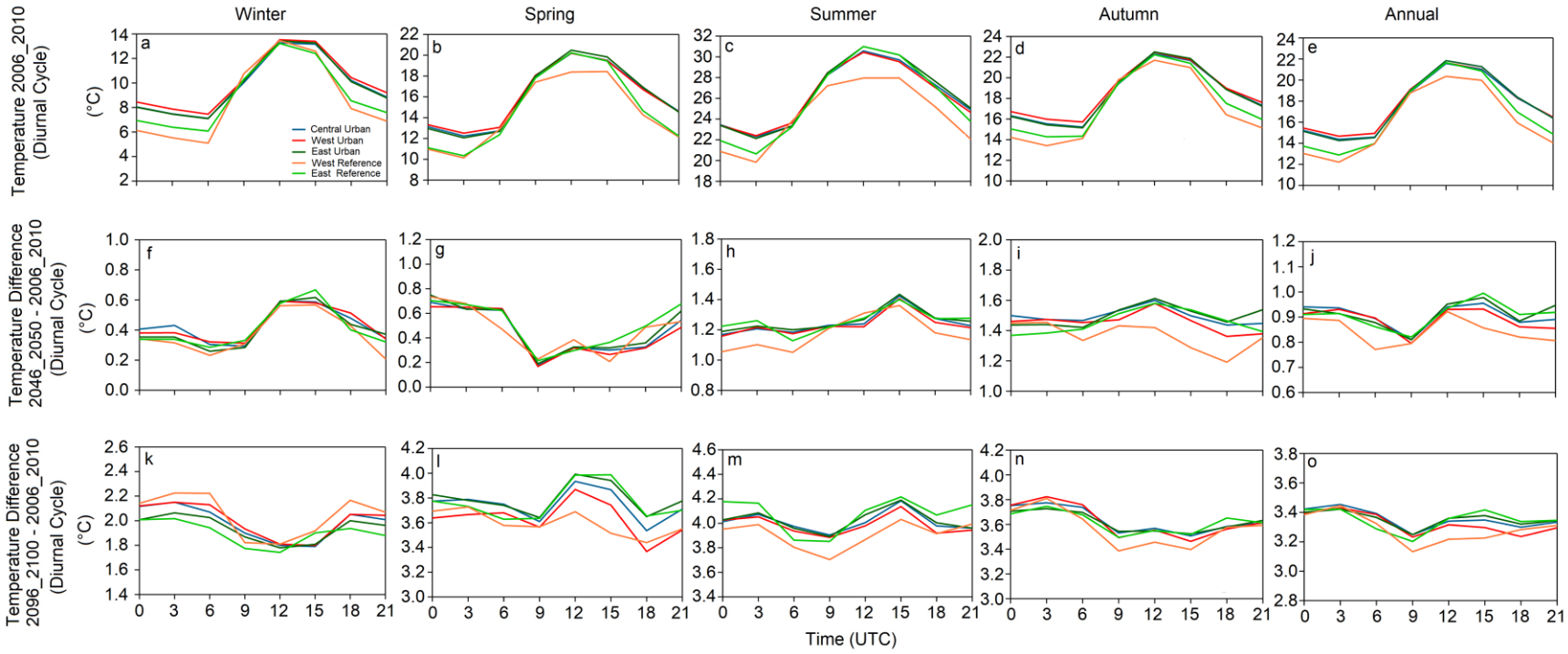

Figure 12 – Figures a-e show the diurnal temperature cycle for the five selected points of the domain of Rome (figure 10). Figures f-j show the temperature difference betweeen the periods 2046-2050 and 2006-2010 for the different seasons of the year. Figures k-o are similar to f-j, but for the periods 2096-2100 and 2006-2010.

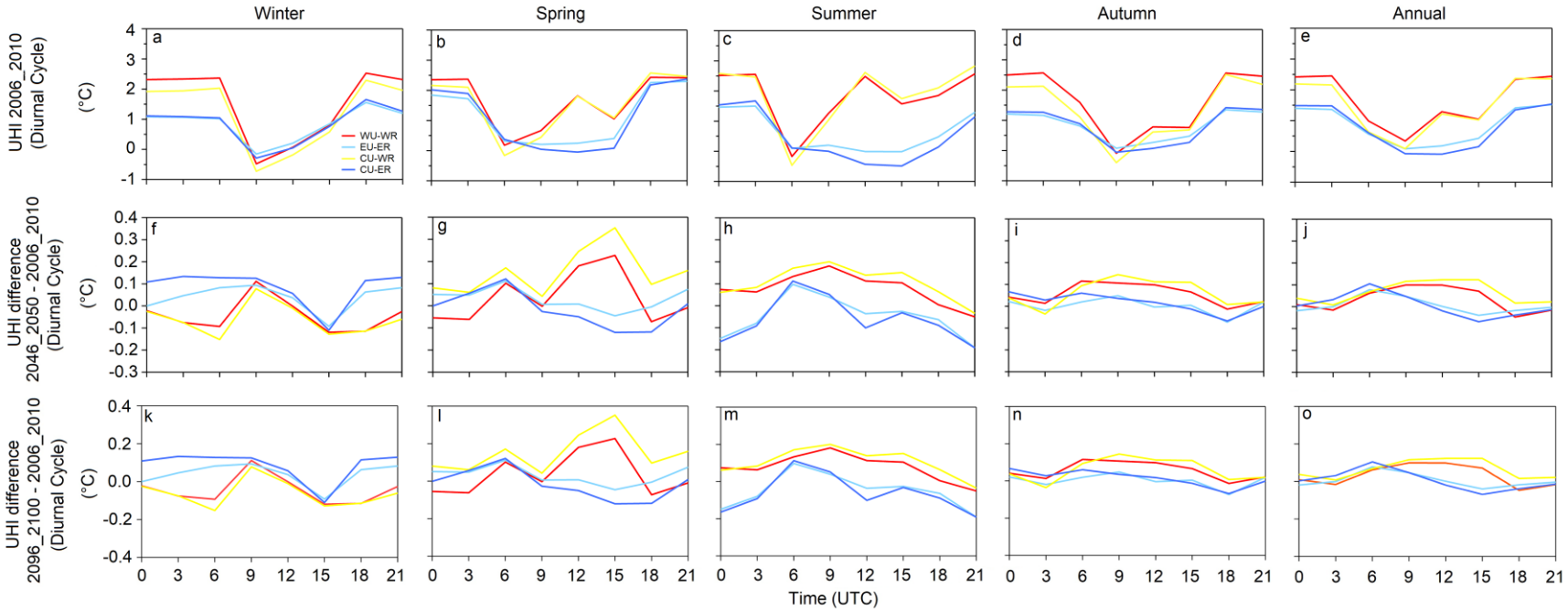

Figure 13 – Figures a-e show the diurnal urban heat island intensity as calculated between WU-WR, EU-ER, CU-WR and CU-ER points of the domain of Rome. Figures f-j show the UHI effect difference for the different seasons of the year betweeen 2046-2050 and 2006-2010. Figures k-o are similar to f-j, but for the periods 2096-2100 and 2006-2010.

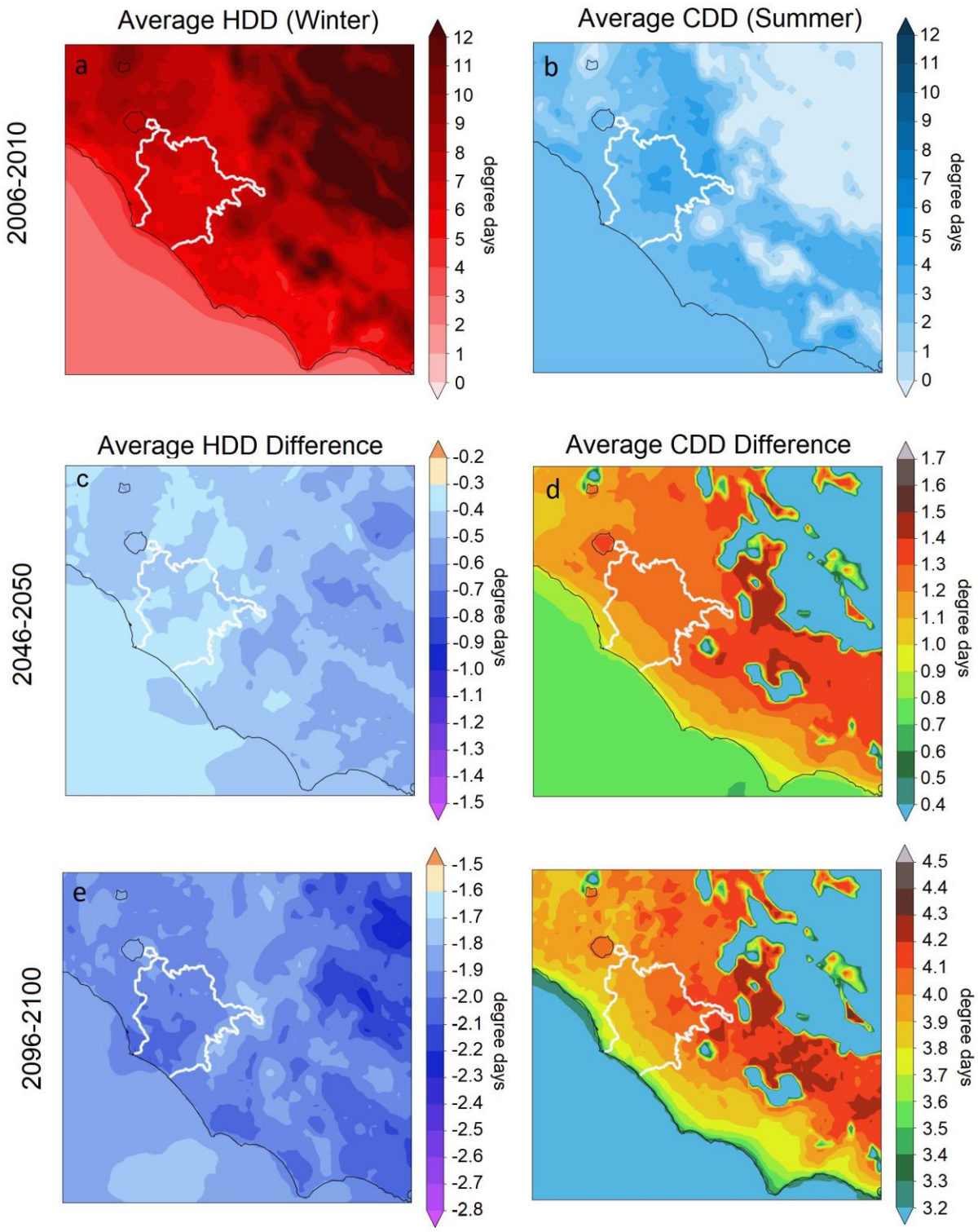

Figure 14 – Same as figure 5, but for domain 04 of Rome.

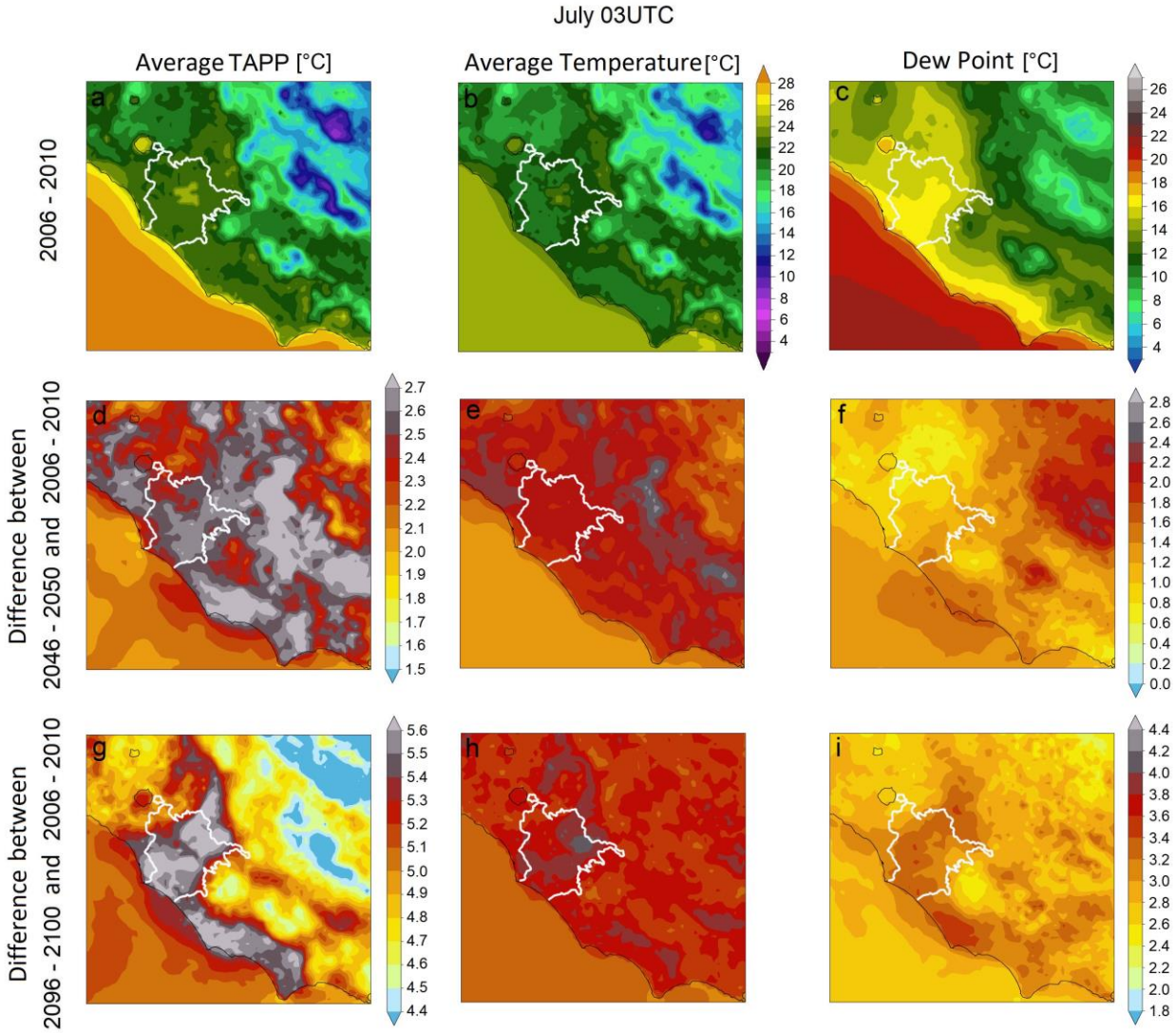

Figure 15 – Same as figure 8, but for domain 04 of Rome.

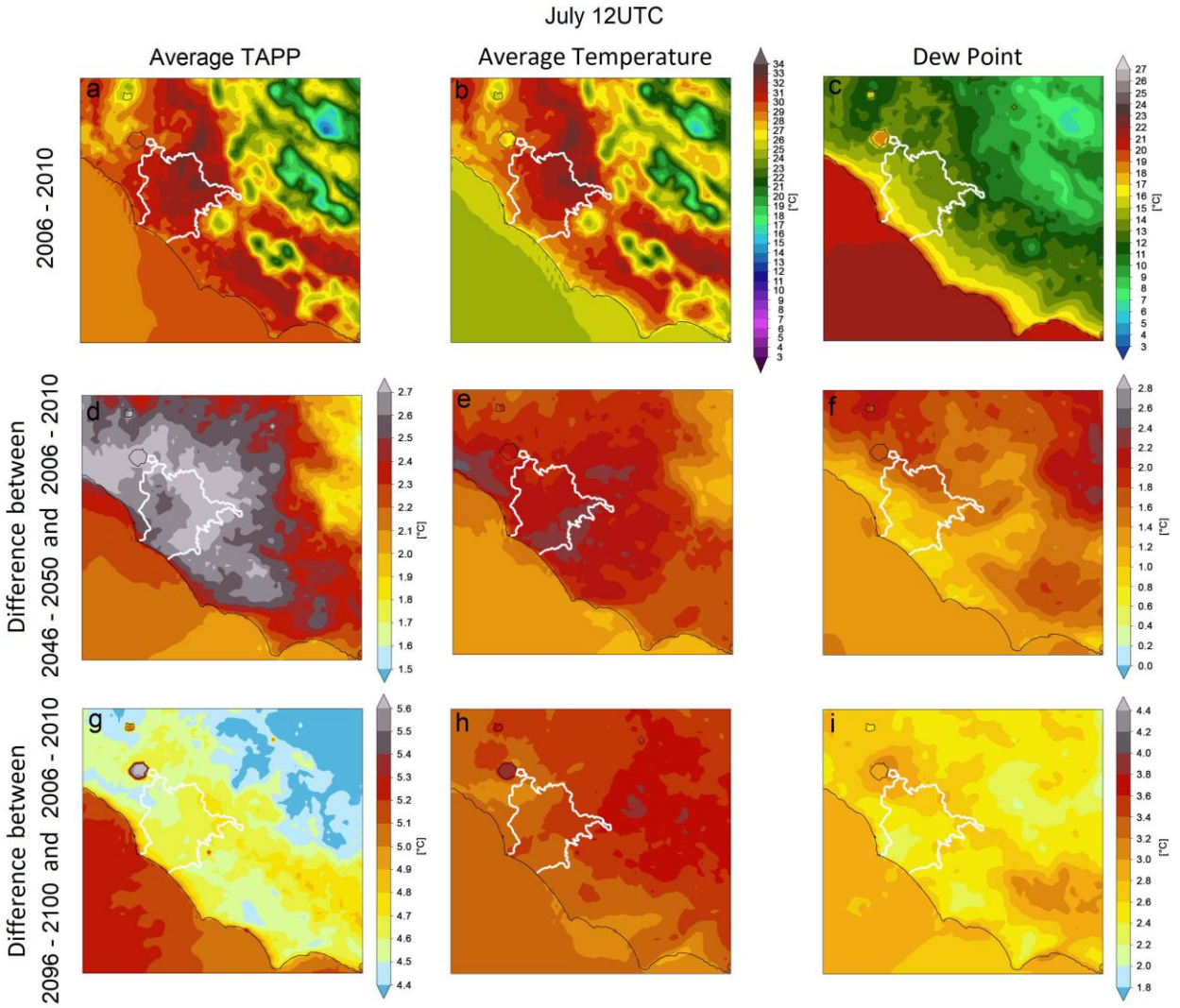

Figure 16 – Same as figure 9, but for domain 04 of Rome.

References

Benmarhnia T, Deguen S, Kaufman JS, Smargiassi A. Review Article: Vulnerability to Heat-related Mortality: A Systematic Review, Meta-analysis, and Meta-regression Analysis. Epidemiology. 2015;26(6):781-793. doi:10.1097/EDE.0000000000000375

Bruyère, Cindy L., et al. "Bias corrections of global models for regional climate simulations of high-impact weather." *Climate Dynamics* 43.7 (2014): 1847-1856.

Büttner, G. (2014). CORINE land cover and land cover change products. In Land use and land cover mapping in Europe (pp. 55-74). Springer, Dordrecht.

Curriero FC, Heiner KS, Samet JM, Zeger SL, Strug L, Patz JA. Temperature and mortality in 11 cities of the eastern United States. Am J Epidemiol. 2002;155(1):80-87. doi:10.1093/aje/155.1.80

Giannaros, C., Nenes, A., Giannaros, T.M., Kourtidis, K., Melas, D., 2018. A comprehensive approach for the simulation of the Urban Heat Island effect with the WRF/SLUCM modeling system: The case of Athens (Greece). Atmos. Res. 201, 86–101. doi:https://doi.org/10.1016/j.atmosres.2017.10.015.

Hong, Song-You, and Jeong-Ock Jade Lim. "The WRF single-moment 6-class microphysics scheme (WSM6)." *Asia-Pacific Journal of Atmospheric Sciences* 42.2 (2006): 129-151.

Hua, T., Zhao, W., Liu, Y., Wang, S., & Yang, S. (2018). Spatial consistency assessments for global land-cover datasets: A comparison among GLC2000, CCI LC, MCD12, GLOBCOVER and GLCNMO. Remote Sensing, 10(11), 1846.

Iacono, Michael J., et al. "Radiative forcing by long-lived greenhouse gases: Calculations with the AER radiative transfer models." *Journal of Geophysical Research: Atmospheres* 113.D13 (2008).

Janjic, Z. I. "The surface layer in the NCEP Eta model. 11th Conf. on Numerical Weather Prediction, Norfolk, VA, 19-23 August 1996." *Amer. Meteor. Soc. Boston, MA* (1996): 354-355.

Joshi, S. S., Lesser, T. J., Olsen, J. W., & O'Hara, B. F. (2016). The importance of temperature and thermoregulation for optimal human sleep. Energy and Buildings, 131, 153-157.

Kain, J.S., 2004. The Kain–Fritsch Convective Parameterization: An Update. J. Appl. Meteorol. 43, 170–181. doi:10.1175/1520-0450(2004)043<0170:TKCPAU>2.0.CO;2.

Kalkstein, L. S., & Valimont, K. M. (1986). An evaluation of summer discomfort in the United States using a relative climatological index. Bulletin of the American Meteorological Society, 67(7), 842-848.

Lan, L., Pan, L., Lian, Z., Huang, H., & Lin, Y. (2014). Experimental study on thermal comfort of sleeping people at different air temperatures. Building and Environment, 73, 24-31.

Lan, L., Tsuzuki, K., Liu, Y. F., & Lian, Z. W. (2017). Thermal environment and sleep quality: A review. Energy and Buildings, 149, 101-113.

Monin, Andreĭ Sergeevich, and Aleksandr Mikhaĭlovich Obukhov. "Basic laws of turbulent mixing in the surface layer of the atmosphere." *Contrib. Geophys. Inst. Acad. Sci. USSR* 151.163 (1954): e187.

Tateishi, Ryutaro, et al. "Production of global land cover data–GLCNMO." International Journal of Digital Earth 4.1 (2011): 22-49.

Tewari, M., Chen, F., Wang, W., Dudhia, J., LeMone, M.A., Mitchell, K., Ek, M., Gayno, G., Wegiel, J., Cuenca, R.H., 2004: Implementation and verification of the unified NOAH land surface model in the WRF model. 20th conference on weather analysis and forecasting/16th conference on numerical weather prediction, pp. 11–15

Wichmann, J., Andersen, Z., Ketzel, M., Ellermann, T., & Loft, S. (2011). Apparent temperature and cause-specific emergency hospital admissions in Greater Copenhagen, Denmark. PLoS One, 6(7), e22904.

The project Implementation of a forecAsting System for urban heat Island effect for the development of urban adaptation strategies- LIFE ASTI has received funding from the LIFE Programme of the European Union".